Applied Catalysis B: Environmental 205 (2017) 393–403

Contents lists available at ScienceDirect

Applied Catalysis B: Environmental

journal homepage: www.elsevier.com/locate/apcatb

Meso-Zr-Al-beta zeolite as a robust catalyst for cascade reactions in biomass valorization

Song Song[a], Lu Di[a], Guangjun Wu[a], Weili Dai[a], Naijia Guan[a,b], Landong Li[a,b,*]

[a] School of Materials Science and Engineering & National Institute for Advanced Materials, Nankai University, Tianjin 300350, PR China
[b] Key Laboratory of Advanced Energy Materials Chemistry of Ministry of Education, Collaborative Innovation Center of Chemical Science and Engineering, Nankai University, Tianjin 300071, PR China

ARTICLE INFO

Article history:
Received 14 November 2016
Received in revised form
11 December 2016
Accepted 23 December 2016
Available online 26 December 2016

Keywords:
Cascade reaction
Biomass valorization
Multifunctional zeolite
Mutual compatibility
Furfural to γ-valerolactone

ABSTRACT

Hierarchical Meso-Zr-Al-beta zeolites are successfully prepared through a multiple-step post-synthesis strategy composed of controlled dealumination, desilicication and metal incorporation. The presence of both Brønsted and Lewis acid sites with a certain extent of strength in Meso-Zr-Al-beta is demonstrated by NH_3-TPD and FTIR spectroscopy with pyridine adsorption/desorption. The creation of mesopores via desilicication through alkaline treatment is confirmed by N_2 adsorption/desorption isotherms. Meso-Zr-Al-beta, with Brønsted acid sites, Lewis acid sites and mesopores, is applied as a zeolite catalyst for the cascade conversion of biomass platform molecule furfural to γ-valerolactone. Owing to the presence of multiple functional sites and their mutual compatibility, remarkable activity for γ-valerolactone production and catalyst recyclability could be achieved with a single Meso-Zr-Al-beta, which appears to be a better catalyst than the commonly-employed combination catalyst systems. The multifunctional Meso-Zr-Al-beta zeolite is also applied as a promising catalyst in other cascade reactions in biomass valorization, i.e. glucose conversion to 5-hydromethylfurfural and trioses conversion to ethyl lactate. Similar zeolite catalysts containing multiple functional sites could be prepared via similar routes, and the number of acid sites and their strength can be adjusted to some extent to derive an optimized catalyst by changing the preparation parameters.

1. Introduction

With increasing demands for the renewable chemicals and fuels, biomass has attracted great attention as an alternative feedstock. In the past decades, extensive researches on the valorization of biomass resources have been motivated [1,2]. Lignocellulose, a key part of biomass, is composed of cellulose, hemicellulose and lignin. Starting from lignocelluose, a lot of valuable platform molecules, such as 2,5-dimethylfuran [3–5], 5-hydromethylfurfural [6,7], furfural [8–10], and γ-valerolactone (GVL) [11,12], can be selectively produced through specific chemical and catalytic processes.

Zeolites are crystalline materials composed of SiO_4 and $[AlO_4]^-$ tetrahedral, well-known as an efficient catalyst in fluid catalytic cracking (FCC) in traditional petrochemical field [13]. In recent years, zeolites have played a more and more important role in the catalytic conversion of biomass, especially in the transformation of bio-derived platform molecules into targeted chemicals [14–16]. Tunable acidity, shape-selective microporous structure and high surface area are recognized as key advantages of zeolite materials applied as catalysts and catalyst supports for biomass conversion. Specifically, water-tolerant Lewis acid zeolites, e.g. Sn-beta [17], have been reported to exhibit extraordinary catalytic activity in bio-derived platform molecules conversion, e.g. glucose isomerization to fructose [18], the production of lactates from carbohydrates [19] and C—C coupling between 1,3-dihydroxyacetone (DHA) and formaldehyde [20]. However, the absence of Brønsted acid sites in Sn-beta zeolite restricts its application in reactions that require both Brønsted and Lewis acid sites. A typical example is the transformation of glucose to 5-hydromethylfurfural, which requires Lewis acid sites to catalyze isomerization of glucose to fructose and Brønsted acid sites to catalyze the subsequent dehydration of fructose to 5-hydromethylfurfural [21]. To overcome the limitations of Sn-beta zeolite, the addition of mineral acids (e.g. HCl, H_2SO_4) or solid Brønsted acids (e.g. Al-MFI, Amberlyst 70) is employed in the reaction. Another classic example reported by Roman Leshkov et al. is the cascade conversion of furfural to γ-valerolactone (GVL) catalyzed by the physical mixture of Lewis acidic Zr-beta and Brønsted acidic Al-MFI [22]. With the help of Brønsted and Lewis acid sites, a high GVL yield of 62% could be obtained after 24 h at 393 K. Likewise,

* Corresponding author at: School of Materials Science and Engineering & National Institute for Advanced Materials, Nankai University, Tianjin 300350, PR China.
E-mail address: lild@nankai.edu.cn (L. Li).

http://dx.doi.org/10.1016/j.apcatb.2016.12.056
0926-3373/

Fan et al. also report that the combination of Au/ZrO_2 and H-ZSM-5 catalysts could effectively catalyze the conversion of furfural to GVL with a high yield of 77.5% [23]. For the combination catalyst systems, the intermediate products have to diffuse or transfer from one catalyst to another, and, theoretically, it is not good to achieve a high yield of target product, especially when zeolites with diffusion problems are employed as catalysts. Recently, Lewis acidic zeolites with varying amounts of Brønsted acid sites have been successfully synthesized [24–30], and also employed as bifunctional catalysts for the cascade conversion of furfural to GVL. For example, Melero et al. report the one-pot conversion of xylose into GVL with considerable yield of 35% at 463 K after 48 h using bifunctional Brønsted-Lewis Zr-Al-beta zeolite as catalyst [31]. Generally, the GVL yields are somewhat lower than combination catalysts systems. For a single zeolite containing both Brønsted and Lewis acid sites, the compatibility of Brønsted and Lewis acid sites should be a key issue influencing its catalytic activity in cascade reactions.

A big challenge for zeolite catalysts using in biomass valorization is its intrinsic microporosity, which might hinder the interaction of bulky bio-derived molecules with active sites and the diffusion of bulky bio-derived molecules [32]. In this context, the construction of hierarchically structur, e.g. mesopores, in zeolite has been proposed to enhance diffusion inside the zeolite crystal and also to increase the number of accessible active sites [33–40]. Thereupon, multifunctional zeolites with of Brønsted-Lewis acid characteristic and hierarchical mesoporous property are expected to be potential catalysts for cascade reactions in biomass valorization. Of course, the mutual compatibility of different functional sites is very important in the construction of multifunctional zeolites.

Inspired by the pioneer work in the literature [41,42] and our previous work on Lewis acidic zeolites [43–47], we herein report the preparation and characterization of a multifunctional zeolite Meso-Zr-Al-beta, containing Brønsted acid sites, Lewis acid sites and mesopores. The Meso-Zr-Al-beta is employed as promising catalyst for one-pot conversion of biomass-derived furfural to GVL. The remarkable catalytic activity in GVL production demonstrates the good mutual compatibility of different functional sites in Meso-Zr-Al-beta, which can also be applied in other cascade reactions, i.e. glucose conversion to 5-hydromethylfurfural and trioses conversion to ethyl lactate.

2. Experimental section

2.1. Chemicals

The following reagents were used in our experiments without further purification: furfural (98%, Alfa), methanol (99%, Alfa), ethanol (99%, Acros), 1-butanol (99%, Alfa), 2-propanol (99%, Alfa), 2-butanol (99%, Alfa), cyclohexanol (99%, Alfa), glucose (99%, Alfa), dimethyl sulfoxide (99%, Alfa), fructose (99%, Alfa), phenol (99%, Alfa), levulinic acid (98%, Alfa), formic acid (97%, Alfa), 5-hydroxymethylfurfural (98%, Acros), 1,4-dioxane (99%, Acros), dichloromethane (99%, Alfa), dihydroxyacetone (Accela, 97%), glyceraldehyde (90%, Sigma), pyruvic aldehyde (40% in water, Acros), ethyl lactate (98%, TCI), dimethyltin dichloride (98%, Alfa), titanocene dichloride (99%, Alfa), zirconocene dichloride (99%, Alfa), oxalic acid (98%, Alfa), ammonium hydroxide(28–30% in water, Alfa).

2.2. Catalyst preparation

Commercial H-beta with an n_{Si}/n_{Al} ratio of 12 (Nankai University) was used for synthesizing metal incorporating beta zeolites. Parent H-beta was first treated with a 0.03 M aqueous $H_2C_2O_4$ (20 mL $g_{zeolite}^{-1}$) at 333 K for 5 h. The mixture was filtered, washed with distilled water until pH = 7, dried at 393 K for 12 h, and further calcined at 823 K for 6 h with 2 K/min heating rate under air to derive a partially dealuminated sample with an n_{Si}/n_{Al} ratio of 23. Afterwards, alkali treatment with aqueous NH_4OH was conducted on the partially dealuminated material to create mesopores. Briefly, 6 g of partially dealuminated H-Beta was dispersed in 120 mL of 0.02 M NH_4OH solution at 333 K for 1.0 h. The slurry was filtered, washed with distilled water until pH = 7, and then dried at 393 K for 12 h. The obtained material was denoted as Meso-beta with an n_{Si}/n_{Al} ratio of 16, which was subjected to acid treatment again with different mole concentrations of oxalic acid solution (1 M, 3 M and 5 M) for 1 h at 353 K to obtain different n_{Si}/n_{Al} ratios of Meso-Al-beta samples. For reference, commercial H-beta material was treated with 13 M HNO_3 solution for 24 h at 353 K to obtain a siliceous microporous beta material, denoted as Si-beta ($n_{Si}/n_{Al} > 1800$).

Zr-containing microporous/mesoporous beta samples were synthesized via post-synthetic strategy, i.e. solid-state metallation, as reported in our previous work [42–44]. Before the incorporation of Zr, the zeolite host was evacuated at 473 K for 12 h to remove the physisorbed water. Then, 0.5 g of the zeolite host powder was finely ground with an appropriate amount of Cp_2ZrCl_2 precursor in the glovebox to achieve an intimate mixture with the n_{Si}/n_{Zr} ratio of 75. The solid mixture was then calcined under static air at 823 K for 6 h with 5 K min^{-1} heating rate to obtain Zr-containing zeolite material. For reference, Ti- and Sn-containing zeolites with a similar n_{Si}/n_{Me} ratio were also prepared via similar procedures, while organometallic precursors Cp_2TiCl_2 and $(CH_3)_2SnCl_2$ were employed instead of Cp_2ZrCl_2 for preparing Ti- and Sn-containing zeolite, respectively. In this work, the metal-containing zeolite samples are labeled as Meso-Me-Al-beta (n_{Si}/n_{Al}-n_{Si}/n_{Me}) or Me-Al-beta (n_{Si}/n_{Al}-n_{Si}/n_{Me}), where Me represents Zr, Ti or Sn. A list of zeolite samples and their preparation procedures are summarized in Table 1.

2.3. Characterization techniques

X-ray diffraction (XRD) patterns of zeolite materials were recorded on a Bruker D8 diffractometer with Cu Kα radiation (λ = 1.54184 Å) from 5° to 35° at a scanning rate of 6°/min.

The silicon, aluminum and zirconium loadings of the zeolite materials were determined by Thermo IRIS Intrepid II XSP atomic emission spectrometer (ICP-AES).

The surface areas and pore volumes of zeolites were measured through nitrogen adsorption at 77 K on a Quantachrome iQ-MP gas adsorption analyzer.

Transmission electron microscopy (TEM) images of Zr-containing zeolite samples were taken on a Tecnai G^2 F20 U-TWIN transmission electron microscope with acceleration voltage of 200 kV.

Diffuse reflectance infrared Fourier transform (FTIR) spectra of zeolite samples were taken on a Bruker Tensor 27 spectrometer with 128 scans at a resolution of 2 cm^{-1}. The samples were pretreated in flowing N_2 at 673 K for 1 h. The spectra were recorded in N_2 against KBr as the background.

FTIR spectra of pyridine adsorption were also conducted on a Bruker Tensor 27 spectrometer. The zeolite samples were placed in a flow cell and evacuated at 673 K for 6 h. After cooling to 298 K, the samples were saturated with pyridine vapor and then evacuated at 473 K, 573 K, or 623 K for 0.5 h. The spectra were recorded at each evacuation temperature in the 4000–650 cm^{-1} range by co-addition of 32 scans.

The temperature-programmed desorption of ammonia (NH_3-TPD) was conducted on Quantachrome ChemBet 3000 chemisorption analyzer. Typically, sample of 0.15 g was pretreated at 873 K for 2 h in He flow, cooled to 353 K and saturated with 5% NH_3/He.

Table 1
Zeolite samples under study and their preparation procedures.

Sample	Acid treatment[a]	Alkali treatment[b]	Acid treatment[c]	Metal incorporation	n_{Si}/n_{Al}	n_{Si}/n_{Me}
H-beta	/	/	/	/	12	/
Meso-beta	0.03 M $H_2C_2O_4$	0.02 M NH_4OH	/	/	16	/
Zr-Al-beta	/	/	2.5 M $H_2C_2O_4$	Cp_2ZrCl_2	100	80
Zr-beta	/	/	13 M HNO_3[d]	Cp_2ZrCl_2	>1800	79
Meso-Zr-Al-beta (49–78)	0.03 M $H_2C_2O_4$	0.02 M NH_4OH	1 M $H_2C_2O_4$	Cp_2ZrCl_2	49	78
Meso-Zr-Al-beta (100-77)	0.03 M $H_2C_2O_4$	0.02 M NH_4OH	3 M $H_2C_2O_4$	Cp_2ZrCl_2	100	77
Meso-Zr-Al-beta (197-78)	0.03 M $H_2C_2O_4$	0.02 M NH_4OH	5 M $H_2C_2O_4$	Cp_2ZrCl_2	197	78
Meso-Zr-Al-beta (97-61)	0.03 M $H_2C_2O_4$	0.02 M NH_4OH	5 M $H_2C_2O_4$	Cp_2ZrCl_2	97	61
Meso-Zr-Al-beta (99–193)	0.03 M $H_2C_2O_4$	0.02 M NH_4OH	5 M $H_2C_2O_4$	Cp_2ZrCl_2	99	193
Meso-Sn-Al-beta (99-77)	0.03 M $H_2C_2O_4$	0.02 M NH_4OH	3 M $H_2C_2O_4$	$(CH_3)_2SnCl_2$	99	77
Meso-Ti-Al-beta (97-76)	0.03 M $H_2C_2O_4$	0.02 M NH_4OH	3 M $H_2C_2O_4$	Cp_2TiCl_2	97	76

[a] 333 K, 5 h.
[b] 333 K, 1 h.
[c] 353 K, 1 h unless specifically stated.
[d] 24 h.

Afterwards, the material was purged with He for 0.5 h to eliminate the physical absorbed NH_3 and NH_3-TPD was then conducted in the range of 353–873 K with 10 K/min heating rate.

Diffuse reflectance ultraviolet-visible (UV–vis) spectra of the dehydrated zeolite samples were measured against $BaSO_4$ in the range of 200–600 nm on a Varian Cary 300 UV–vis spectrophotometer.

X-ray photoelectron spectra (XPS) of the materials were taken on a Kratos Axis Ultra DLD spectrometer with a monochromated Al-Kα X-ray source ($h\nu$ = 1486.6 eV), hybrid (magnetic/electrostatic) optics and a multi-channel plate and delay line detector (DLD).

The quantitative analysis of organic deposited on zeolite catalyst after furfural-to-GVL conversion was performed on a Thermal Advantage Q600 SDT system. Typically, 0.01 g of catalyst sample after five recycles was pretreated at 373 K to remove the physisorbed water/organic and then heated to 1273 K with a rate of 10 K/min in flowing air (20 mL/min). Meanwhile, the temperature-dependent thermogravimetric (TG) curve was recorded.

The nature of bulky reagents deposited on zeolite catalyst after furfural-to-GVL conversion was investigated by dissolution-extraction analysis. In a typical experiment, sample of 0.1 g was dissolved in 4 mL HF solution. The bulky reagents were extracted by 4 mL CH_2Cl_2 (the residual water removed by sodium sulfate solid) and analyzed by gas chromatography-mass spectrometer (Shimadzu GC–MS QP2010 SE, HP-5 column).

2.4. Catalytic evaluation

2.4.1. One-pot conversion of furfural to GVL

The catalytic conversion of furfural was performed in a 25 mL autoclave reactor equipped with a magnetic stirrer (800 rpm) and electronic heater under atmospheric pressure. Typically, 0.12 g catalyst was added into 10 mL of 0.05 M furfural solution (2-propanol as solvent and hydrogen donor) and then the reactor was heated to 393 K and kept for certain time. After the reaction, the autoclave reactor was quickly cooled down to below 298 K. The reaction mixture was analyzed by taking out aliquots of the samples, separating the catalyst, and injecting the liquids to a Shimadzu GC 2010 (Agilent HP-5MS column). The product yield was determined by using decane as an internal standard.

Recycling test was also conducted. Typically, the mixture was centrifuged at 8000 rpm to deposit the solid catalyst after reaction, which was washed with 2 mL of CH_2Cl_2 for five times. Then, the catalyst was dried at 373 K for 12 h for next reuse.

2.4.2. Glucose conversion to 5-hydroemthylfurfural

The catalytic conversion of glucose was performed in a 300 mL autoclave reactor equipped with a magnetic stirrer (800 rpm) and electronic heater. In a typical reaction, 0.5 g catalyst, 20 mL glucose aqueous solution (10 wt.%) and 80 mL dimethyl sulfoxide were added into the reactor under stirring, and then the reactor was heated to 433 K and kept for certain time. The reaction mixture was analyzed using gas chromatography (GC, Shimadzu GC-2010, HP-FAAP column) and high-performance liquid chromatography (HPLC, Shimadzu LC-20A, Aminex HPX-87H column) with refractive index detectors. 5-HMF, LA, and formic acid (FA) were determined using GC and quantified using phenol as an internal standard. The disappearances of glucose and fructose were monitored with HPLC equipped with an Aminex HPX-87H column, using 75:25 v/v acetonitrile: water at a flow rate of 1 mL min^{-1} and a column temperature of 298 K.

2.4.3. Triose conversion of ethyl lactate

The catalytic conversion of triose was performed in a 15 mL autoclave reactor equipped with a magnetic stirrer (800 rpm) and electronic heater. Typically, 75 mg catalyst powder was added to 1 mmol triose in 2.5 mL ethanol, and then the reactor was heated to 363 K and kept at this temperature for certain time. Aliquots of sample were quantitatively analyzed by Shimadzu GC 2010 (Agilent, HP-1 column). Identification of reaction products was achieved according to the retention time analysis and confirmed by GC–MS (Shimadzu GC–MS QP2010 SE, HP-1 column). Quantitative analysis was achieved with 1, 4-dioxane as the internal standard.

3. Results and discussion

3.1. Fabrication of Meso-Zr-Al-beta

According to the recent work of Sels et al. that tunable mesopores of 2–6 nm could be created in USY zeolite upon treatment with NH_4OH aqueous solution [40], a diluted NH_4OH solution was used as the desilication reagent in our study to create mesopores in H-beta zeolites. Fig. 1(left) depicts the XRD patterns of parent H-beta, Meso-beta, Meso-Al-beta and Meso-Zr-Al-beta (100-77) zeolites. All samples show similar diffraction peaks corresponding to BEA topology, demonstrating the preservation of beta zeolite framework upon dealumination, desilication and Zr incorporation. Likewise, no diffraction peaks corresponding to bulky zirconia could be observed due to the low loading or the good dispersion of Zr species in zeolite. It has been reported that dealumination and metal incorporation processes should be accompanied by the contraction/expansion of the zeolite framework, which is reflected by the changes in the position of (302) diffraction peak at $2\theta = \sim 22.5^\circ$ [41,42]. As shown in Fig. 1, 2θ value of (302) diffraction peak in H-beta zeolite increases from 22.42 to 22.65° with desilication-dealumination process, then it decreases to 22.46°

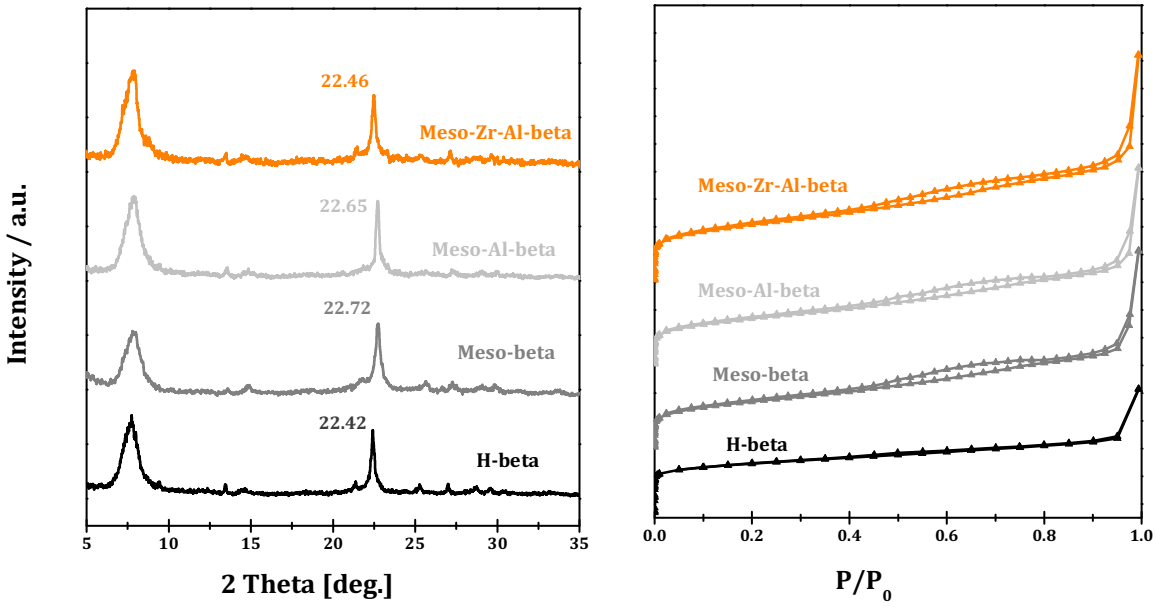

Fig. 1. XRD patterns (left) and N_2 adsorption-desorption isotherms (right) of selected zeolite samples.

Table 2
Physicochemical properties of zeolite samples under study.

Sample	Surface area ($m^2\ g^{-1}$)		Pore volume ($cm^3\ g^{-1}$)	
	S_{BET} [a]	S_{meso}	V_{micro} [b]	V_{meso}
H-beta	563	128	0.20	0.12
Meso-beta	702	401	0.17	0.42
Zr-Al-beta	585	133	0.19	0.12
Zr-beta	600	140	0.19	0.12
Meso-Zr-Al-beta (49–78)	707	405	0.16	0.43
Meso-Zr-Al-beta (100-77)	708	407	0.16	0.44
Meso-Zr-Al-beta (197-78)	710	409	0.15	0.45
Meso-Zr-Al-beta (97-61)	701	399	0.15	0.43
Meso-Zr-Al-beta (99–193)	711	408	0.16	0.44
Meso-Sn-Al-beta (99-77)	715	406	0.15	0.43
Meso-Ti-Al-beta (97-76)	714	405	0.15	0.44

[a] Calculated from BET method.
[b] Calculated from t-plot.

after Zr incorporation. Therefore, XRD results roughly demonstrate the incorporation of zirconium species into the framework of beta zeolite.

Fig. 1 (right) shows the N_2 adsorption and desorption isotherms of the H-beta, Meso-beta, Meso-Al-beta and Meso-Zr-Al-beta (100–77) samples. Parent H-beta zeolite exhibits a typical type I adsorption-desorption isotherm for microporous zeolite. In contrast, the appearance of characteristic hysteresis loop at the relative pressure P/P_0 of 0.4–0.8, a type IV adsorption-desorption isotherm, could be observed for samples with alkaline treatment, i.e. Meso-beta and Meso-Al-beta [48]. Further incorporation of Zr species into Meso-Al-beta zeolite does not change the shape of adsorption-desorption isotherm. These results indicate the successful fabrication of hierarchical mesoporous/microporous structure in Meso-Zr-Al-beta (100–77) sample.

Table 2 summarizes the physicochemical properties of zeolite samples under study. Parent H-beta sample possesses a total surface area of 563 $m^2\ g^{-1}$, with micropore volume of 0.20 $cm^3\ g^{-1}$ and a mesopore volume of 0.12 $cm^3\ g^{-1}$ (caused by the accumulation of nanoparticles). H-beta, Zr-beta and Zr-Al-beta exhibit similar BET surface area (563–600 $m^2\ g^{-1}$) and micropore volume (0.19-0.20 $cm^3\ g^{-1}$), indicating the good preservation of BEA topology after dealumination and Zr incorporation. On the other hand, treatment on H-beta with diluted NH_4OH aqueous solution results in significant increases in the total surface area (from 563 to >700 $m^2\ g^{-1}$) and mesopore volume (from 0.12 to >0.40 $cm^3\ g^{-1}$), accompanied by a slight decrease of micropore volume (from 0.20 to 0.15–0.17 $cm^3\ g^{-1}$). These results clearly confirm the creation of mesopores in microporous beta zeolites upon NH_4OH treatments (Table 2).

According to our previous work [43–46], the incorporation of metal ions into zeolite framework could be monitored by means of infrared spectroscopy. As shown in the FTIR transmittance spectra (Fig. 2, **left**), a new band centered at 950 cm^{-1} appears for Meso-beta compared to the parent H-beta, which should be assigned to defect silanols from dealumination [49]. This band also exists in the sample of Meso-Al-beta. After Zr incorporation, the band at 950 cm^{-1} disappears while a new band centered at 962 cm^{-1} appears. The new FTIR band is assigned to an asymmetric stretching mode of O_3Si-O-Zr group, which is generally recognized as a sign of metal incorporation into zeolite framework [50]. The changes in the hydroxyl stretching vibrations during the fabrication of Meso-Zr-Al-beta are further monitored by diffuse reflection FTIR spectroscopy (Fig. 2, **right**). For the parent H-beta, extra-framework Al-OH groups (3776 cm^{-1}), isolated Si—OH groups (3738 cm^{-1}), isolated terminal Si—OH groups (3660 cm^{-1}) and hydrogen-bonded Si-OH groups (at 3520 cm^{-1}) could be clearly distinguished [51]. After desilicication-dealumination, the band due to isolated Si-OH groups shifts slightly to lower wavenumber (3738–3730 cm^{-1}) and a new band centered at 3520 cm^{-1} originated from the defect silanols appears for Meso-Al-beta. Subsequent Zr incorporation results in the sharp decline of FTIR band at 3520 cm^{-1}, indicating the interaction of Zr species with the Si-OH groups located in the vacant T-atom sites. On the basis of FTIR transmittance spectra and diffuse reflection FTIR spectra of hydroxyl stretching vibrations, we can say that Zr species have been successfully incorporated into beta zeolite via the solid-state metallation route, in good agreement with XRD analysis results (Fig. 1).

3.2. Existing states of Zr in Meso-Zr-Al-beta

The distribution of Zr species in Meso-Zr-Al-beta (100–77) can be directly observed by microscopy analysis (Fig. 3). As shown in the TEM image, Meso-Zr-Al-beta samples appear as ~200 nm aggregations of nanorods or nanosheets. The high-resolution TEM

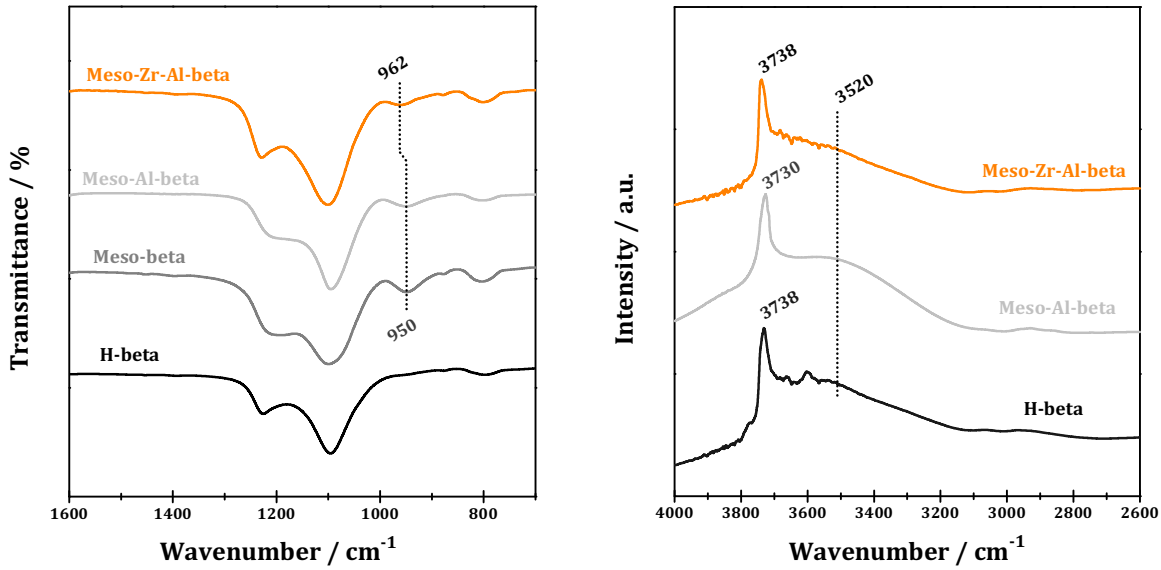

Fig. 2. FTIR transmittance spectra of the skeletal vibrations (left) and diffuse reflection FTIR spectra of the hydroxyl stretching vibrations (right) of selected zeolite samples.

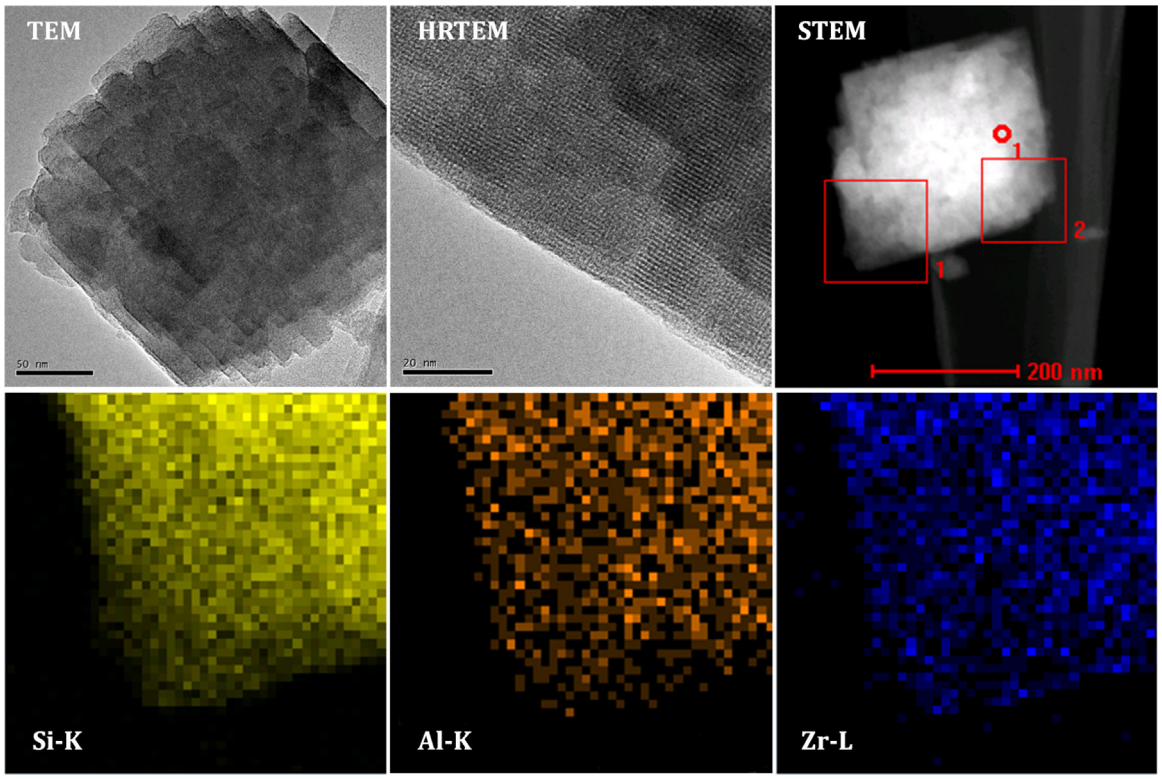

Fig. 3. TEM, HRTEM and STEM images of Meso-Zr-Al-beta (100–77) with corresponding element mapping analysis (Si, Al and Zr).

(HRTEM) image of sample shows the clear lattice fringes of beta zeolite, corresponding to its high crystallinity as revealed by XRD analysis. Meanwhile, some bright region without lattice fringes can be observed due to the existence mesopores. The scanning TEM image (STEM) with corresponding element mapping analysis further confirm the homogeneous dispersion of Zr and Al species in as-prepared Meso-Zr-Al-beta sample. In fact, both Zr and Al species appear to be well-isolated and even dispersed in the atomic level.

UV–vis spectroscopy can provide us with information on the chemical environment of Zr species within zeolite framework [52–54]. For bulk ZrO_2 sample, two bands centered at 205 and 230 nm are observed (Fig. 4, left), which are attributed to the charge transfer from Zr—O—Zr bands. While for all Zr-containing zeolite samples, a dominating band centered at 205 nm is observed, ascribable to the ligand-to-metal charge transfer from O^{2-} to tetrahedral Zr^{4+} ions [52]. The absence of significant band at 230 nm excludes the existence of bulk ZrO2 in Zr-containing zeolite samples. In a whole, the UV–vis spectra indicate that most Zr species have been incorporated in beta zeolite framework with tetrahedral coordination, which are expected to be catalytically active Lewis acid sites.

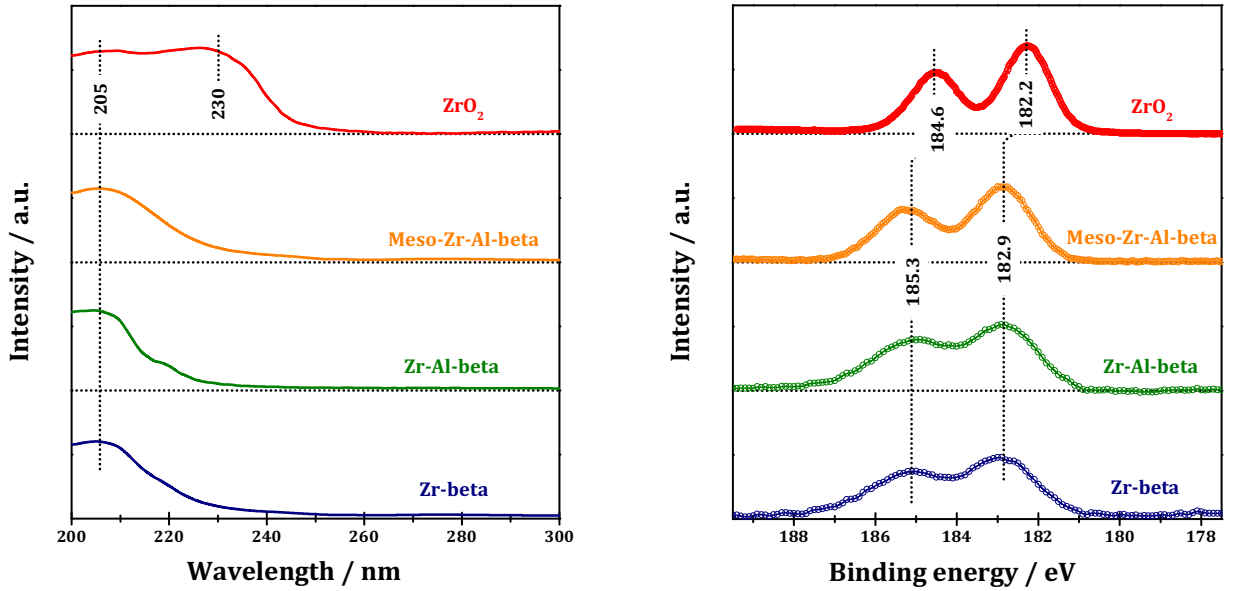

Fig. 4. UV–vis spectra (left) and Zr 3d XPS (right) of selected Zr-containing samples.

Zr 3d XPS of selected Zr-containing samples are measured to provide information on the electronic states of Zr species. In the spectrum of reference bulk ZrO_2 sample (Fig. 4, right), two binding energy values at 182.2 and 184.6 eV, corresponding to Zr $3d_{5/2}$ and $3d_{3/2}$, are observed. While for Zr-containing zeolite samples, i.e. Zr-beta, Zr-Al-beta and Meso-Zr-Al-beta, similar binding energy values at 182.9 (Zr $3d_{5/2}$) and 185.3 eV (Zr $3d_{3/2}$) are observed. These binding energy values are always explained as the framework Zr species in literature reports [45,55–57]. Due to the lower electronegativity of Zr compared to Si, Zr ions should be more positively charged in Zr—O—Si bands than Zr—O—Zr bands, and, therefore, higher Zr 3d binding energy values are observed for Zr species incorporated in zeolite framework. Besides, the presence of Al species in the zeolite samples does not change the existing state of Zr species at all (Zr-beta vs Zr-Al-beta).

3.3. Acidic properties of Meso-Zr-Al-beta

The acidic properties of Meso-Zr-Al-beta and reference samples are evaluated by means of NH_3-TPD and FTIR spectra of pyridine adsorption.

NH_3-TPD is first employed to analyze the amount and strength of acid sites in samples and the NH_3-TPD profiles are shown in Fig. 5. Parent H-beta zeolite exhibits a wider temperature range of NH_3 desorption from 400 to 900 K, and the two desorption peaks centered at 503 and 643 K reveal the presence of both weak and strong acid sites. For Zr-beta zeolite (Si/Zr = 79), two peaks centered at 453 and 563 K can be observed due to ammonia desorption from weak and medium acid sites. Obviously, the absence of framework Al species greatly reduces the strength of acid sites in beta zeolite. While for hierarchical Meso-Zr-Al-beta (100–77) zeolite, two ammonia desorption peaks at 503 and 613 K can be observed, corresponding to the weak and strong acid sites, respectively. It is noted that the density of weak acid sites in Meso-Zr-Al-beta zeolite is slightly lower than that in H-beta (0.35 vs 0.38 mmol g^{-1}), while the density of strong acid sites is higher (0.69 vs 0.62 mmol g^{-1}). That is, the loss of acid sites due to the removal of framework Al species could be well compensated by the incorporation of Zr species into zeolite framework.

The Brønsted and Lewis acidity of Meso-Zr-Al-beta (100–77) is analyzed by FTIR spectroscopy of pyridine adsorption/desorption,

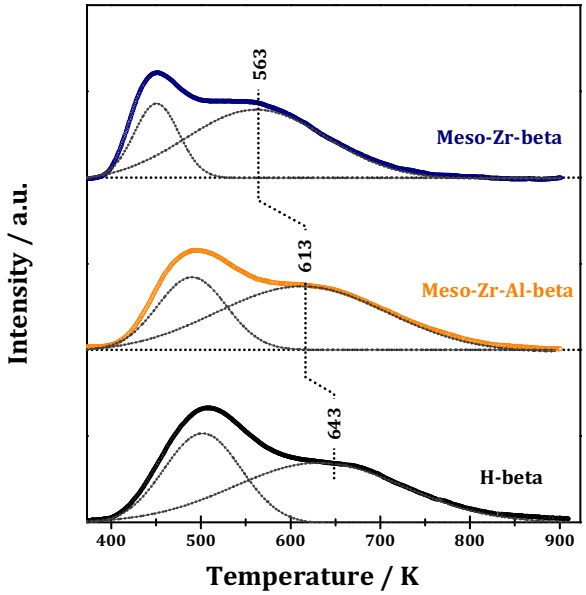

Fig. 5. NH_3-TPD profiles of H-beta, Meso-Zr-beta (79) and Meso-Zr-Al-beta (100–77) samples.

and the results are shown in Fig. 6. Generally, pyridine molecules adsorption on the Lewis acid sites of sample gives rise to the FTIR-active bands at 1450, 1490 and 1610 cm^{-1}, while pyridine molecules adsorption on the Brønsted acid sites of sample gives rise to bands at 1490, 1550 and 1640 cm^{-1} [58,59]. All these FTIR bands can be observed for Meso-Zr-Al-beta (100-77) sample after pyridine adsorption and evacuation at 473 K, indicating the presence of both Brønsted and Lewis acid sites. The Brønsted acid sites should come from the existence of framework Al species and the Lewis acid sites from framework Zr species. With increasing evacuation temperature, pyridine molecules start to desorb from the acid sites in the sample, as reflected by the decrease in the corresponding FTIR band intensity (both Brønsted and Lewis acid sites). After evacuation at 623 K, no pyridine molecules interacting with Brønsted acid sites can be observed any more, while a significant amount of pyridine molecules interacting with Lewis acid sites are still preserved.

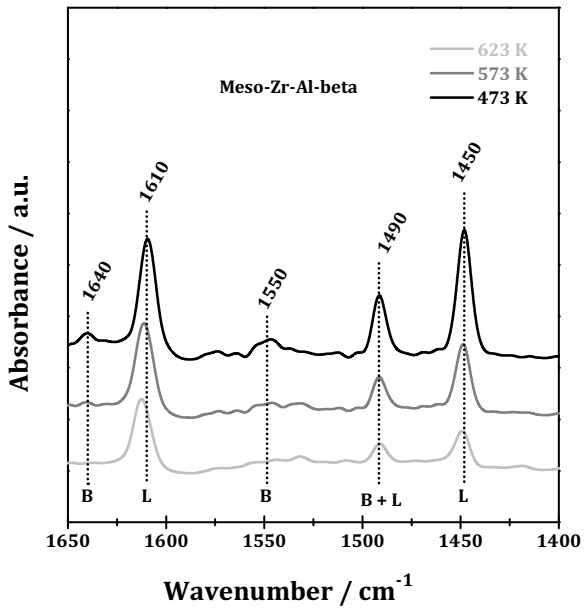

Fig. 6. FTIR spectra of Meso-Zr-Al-beta (100–77) sample after pyridine adsorption and evacuation at different temperatures.

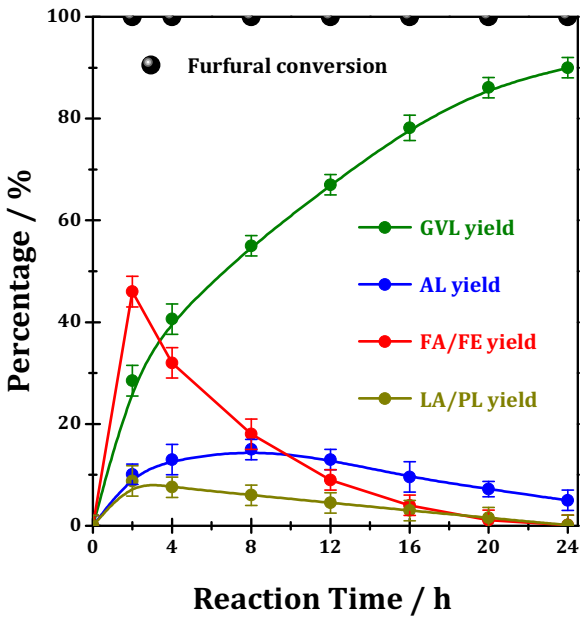

Fig. 7. Time course of one-pot catalytic conversion of furfural to GVL over Meso-Zr-Al-beta (100–77). Reaction conditions: 0.12 g catalyst, 0.05 M furfural in 10 mL 2-propanol, T = 393 K.

These results confirm the presence of strong Lewis acid sites in Meso-Zr-Al-beta (100-77) sample and quantitative analysis indicates strong Lewis acid sites of 0.28 mmol g^{-1} among overall Lewis acid sites of 0.89 mmol g^{-1}.

3.4. Catalytic properties of Meso-Zr-Al-beta

3.4.1. One-pot conversion of furfural to γ-valerolactone

On the basis of literature report [22,60–63] and our own experimental observations, the reaction network for the one-pot conversion of furfural to GVL is depicted in Scheme 1. In the first step, the catalytic transfer hydrogenation (CTH) of furfural to furfural alcohol (FA) and its ether (FE) can be achieved with Lewis acid sites in the presence of 2-propanol as hydrogen donor. In the second step, the hydrolytic ring-opening of furfural alcohol and its ether to levulinic acid (LA) and its ester (PL) can be achieved with Brønsted acid sites. In the last step, Lewis acid sites enable CTH of LA/PL to produce the corresponding 4-hydroxypentanoates, followed by lactonization to the target product GVL. Alternatively, LA can be dehydrated to pseudo-levulinic acid, which undergoes further dehydration to angelica lactone. The angelica lactone can be converted to GVL on Lewis acid sites via CTH process.

Fig. 7 depicts the time course of furfural conversion catalyzed by Meso-Zr-Al-beta (100-77). The conversion of furfural quickly reaches 100% within 1 h. FA/FE from CTH of furfural on Lewis acid sites is observed as the dominating intermediate product at the initial stage of reaction (within 2 h), and the hydrolysis product from FA/FE on Brønsted acid sites, i.e. LA/PL, can also be observed. With the further progress of reaction, the yields of both FA/FE and LA/PL decrease gradually, while the yield of GVL increases instead, indicating the transformation of LA/PL to GVL via CTH and lactonization (on Lewis acid sites). In our experimental, GVL yield can reach 90% after 24 h (Angelica lactone is observed as by-product because the CTH of angelica lactone to GVL is kinetically slow). To our knowledge, this is the best results for GVL production from furfural under similar reaction conditions, especially using a single catalyst system. Roman et al. has reported that carbon balance increased to 77% within 24 h, and finally to 87% at 48 h with prolonging reaction time for the one-pot conversion of furfural to GVL, and the carbon loss should be due to the formation oligomeric species in the zeolite pores. In our experiments, carbon balance of as high as 96% can be obtained after reaction for 24 h over Meso-Zr-Al-beta (calculated from the all detectable carbon species) owing to the presence of hierarchical pores that can increase the diffusion of product and suppress the formation of oligomeric species. The unique properties of hierarchical Meso-Zr-Al-beta are good for catalyst recycling (vide infra) and potential application. Moreover, di-isopropyl ether can be detected in the reaction system from the etherification of 2-propanol solvent, while the amount of di-isopropyl ether is very low (less than one-tenth of GVL) due to low reaction temperature employed.

To achieve an in-depth understanding on the conversion of furfural to GVL catalyzed by different types of acid sites, a series of solid acids are employed in the reaction and the results are summarized in Table 3. H-beta with both Brønsted and Lewis acid sites cannot effectively catalyze the conversion of furfural to GVL, and LA/PL is observed as the dominating product (**Entry 1**). Obviously, the Lewis acid sites in H-beta are not strong enough to effectively catalyze the transfer hydrogenation of LA/PL although they can catalyze the transfer hydrogenation of furfural. That is, stronger Lewis acid sites are required for the CTH of LA/PL than furfural. When Zr-beta with only Lewis acid sites is employed in the conversion of furfural, FA/FE is obtained as the exclusive product (**Entry 2**) because the further conversion of FA/FE requires Brønsted acid sites. If some of the framework Al species are preserved during the dealumination process, i.e. through controlled partial dealumination, some Brønsted acid sites can be preserved and the as-prepared Zr-Al-beta with both Brønsted and Lewis acid sites can catalyze the conversion of furfural to GVL (**Entry 3–5**). It should be mentioned that the density of Brønsted acid sites in Zr-Al-beta can influence the product distribution from furfural conversion, and, with similar Si/Zr ratio of ~80, a Si/Al ratio of ~100 is optimized for Zr-Al-beta. Compared with the combination catalyst of Brønsted acids and Lewis acids employed in the reaction, e.g. Zr-beta and H-ZSM-5, the use of a single catalyst containing both Brønsted and Lewis acid sites in our study is expected to show advantages in the diffusion of intermediate products. In principle, all the steps of cascade reaction can occur within the cages of Zr-Al-beta catalyst and the intermediate products, i.e. FA/FE and LA/PL, do not need

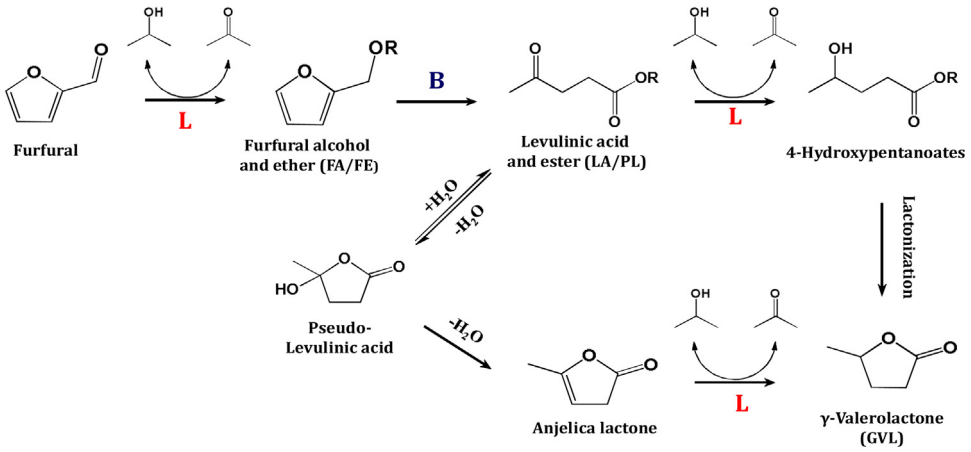

Scheme 1. Reaction network for furfural conversion to γ-valerolactone.

Table 3
One-pot catalytic conversion of furfural to GVL over various zeolites[a].

Entry	Catalyst	n_{Si}/n_{Al} ratio[b]	n_{Si}/n_{Me} ratio[b]	Water/vol%[c]	Yield/mol%[d]				Carbonbalance
					FA/FE	LA/PL	AL	GVL	
1	H-beta	12.5	/	0	0	67	14	2	85%
2	Zr-beta	>1800	79	0	97	0	0	0	97%
3	Zr-Al-beta	48	80	0	0	30	11	42	84%
4	Zr-Al-beta	96	79	0	0	2	5	71	79%
5	Zr-Al-beta	194	77	0	8	11	13	50	82%
6	H-beta Zr-beta	100 >1800	/ 79	0	0	13	12	35	70%
7	Meso-Zr-Al-beta	49	78	0	0	22	15	61	98%
8	Meso-Zr-Al-beta	100	77	0	0	0	2	90	96%
9	Meso-Zr-Al-beta	197	78	0	0	17	13	57	90%
10	Meso-Zr-Al-beta	97	61	0	0	1	2	90	94%
11	Meso-Zr-Al-beta	99	193	0	0	19	12	54	89%
12	Meso-Sn-Al-beta	99	77	0	0	2	34	51	87%
13	Meso-Ti-Al-beta	97	76	0	0	36	21	29	89%
14	Meso-Zr-Al-beta	100	77	5	0	0	1	95	96%
15	Meso-Zr-Al-beta	100	77	10	0	0	3	91	94%
16	Meso-Zr-Al-beta	100	77	15	0	0	5	88	93%

[a] Reaction conditions: 0.12 g catalyst, 0.05 M furfural, 10 mL 2-propanol with or without water, T = 393 K.
[b] Determined by ICP analysis.
[c] Water content in solvent.
[d] After reaction for 24 h.

to take a long journey to diffuse out of and into the zeolite cages as required for the combination catalyst systems. In fact, Zr-Al-beta catalyst (**Entry 4**) exhibits distinctly higher catalytic activity for furfural to GVL conversion than the combination of H-beta and Zr-beta with similar acidity (**Entry 6**) and under identical reaction conditions, confirming the advantages of using a single catalyst instead of combination catalyst system. It is known that the creation of hierarchical structure in zeolite catalysts can promote the accessibility of active sites and increase the diffusion of reactant and products, which accordingly improve the catalytic activity and suppress the catalyst deactivation [45]. Herein, mesopores are created in Zr-Al-beta via a desilication process induced by alkane treatment and the as-prepared Meso-Zr-Al-beta zeolites are employed in the cascade conversion of furfural to GVL. It is shown that Meso-Zr-Al-beta zeolites (**Entry 7–9**) exhibit higher activity for GVL production than Zr-Al-beta with similar Si/Al and Si/Zr ratios (**Entry 3–5**). These observations clearly demonstrate the advantages of catalyst hierarchical structure in the reaction. We also prepare hierarchical Meso-Sn-Al-beta and Meso-Ti-Al-beta zeolites via similar route, and they appear to be active catalysts for furfural conversion with GVL yield of 51 and 29%, respectively (**Entry 12&13**). The lower activity of Meso-Sn-Al-beta and Meso-Ti-Al-beta as compared to Meso-Zr-Al-beta should be originated from their lower Lewis acid strength, in agreement with previous report [22].

With Meso-Zr-Al-beta as model multiple functional catalysts, we further investigate the effect of Brønsted/Lewis acid ratios on the conversion of furfural to GVL. As shown in Fig. 8, the normalized GVL productivity (in the unit of $mol_{GVL}mol_{acid}^{-1}h^{-1}$) is dependent on the Brønsted/Lewis acid ratio. Since the cascade conversion of furfural to GVL is catalyzed by Lewis, Brønsted and Lewis acid sites step by step, a balance between Brønsted and Lewis acid sites is required to efficiently catalyze the reaction. Here, a Brønsted/Lewis acid ratio of ~0.5, i.e. Meso-Zr-Al-beta (100–77), is optimized for the reaction.

Since water is inevitable in practical biomass conversion, it is important to investigate the effect of water content on the catalytic conversion of furfural to GVL. It is seen that addition of 5% water in the reaction system results in a noticeable increase in GVL yield from 90 to 95% (**Entry 14**), which can be explained from the promoted hydrolysis of FA/FE to LA/BL by water. While with further increase in the water content from 5 to 15%, a slight decrease in GVL yield from 95 to 88% can be observed (**Entry 15&16**). The loss of catalytic activity might be due to the change of pore hydrophobicity in Meso-Zr-Al-beta with increasing water content.

On the basis of the above-mentioned results, it is clear that Brønsted acid sites, Lewis acid sites and hierarchical mesopores can be integrated into a single zeolite with mutual compatibility, which is applied as a robust catalyst for the cascade conversion of

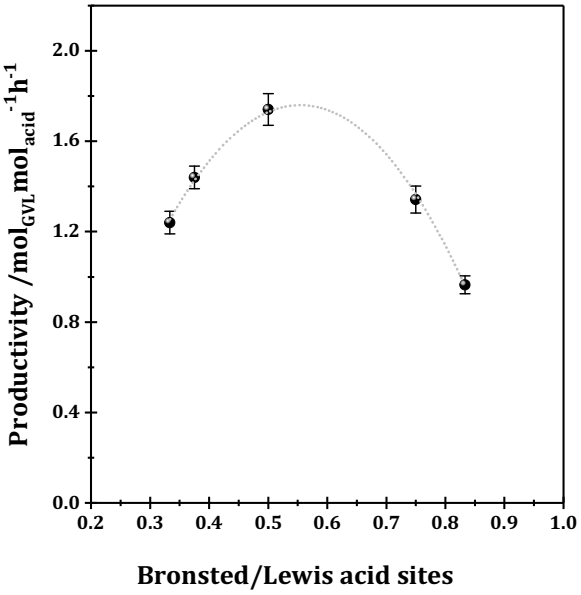

Fig. 8. Normalized GVL productivity of Meso-Zr-Al-beta as a function of Brønsted/Lewis acid ratio.

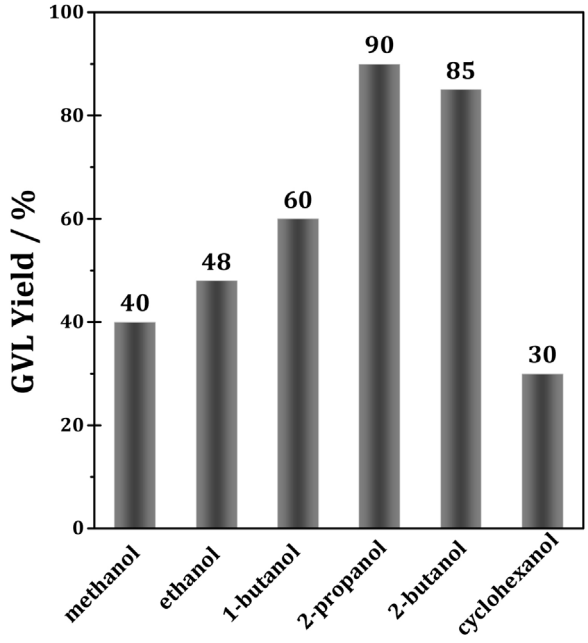

Fig. 9. One-pot catalytic conversion of furfural to GVL with various alcohols as the hydrogen donors. Reaction conditions: 0.12 g Meso-Zr-Al-beta, 0.05 M furfural, 10 mL alcohol as the hydrogen donor, T = 393 K, 24 h.

furfural to GVL. The number of Brønsted/Lewis acid sites (Si/Al and Si/M ratios) and the strength of Lewis acid sites (types of metal incorporated into zeolite framework) can be adjusted by changing preparation parameters. For the optimized catalyst Meso-Zr-Al-beta (100–77), the highest GVL yield of 95% could be obtained, which appears to be the best results ever reported under comparable reaction conditions [22,23].

Hydrogen donors play an important role in the CTH reaction [64,65]. Considering that the cascade conversion of furfural to GVL involves two steps of CTH reaction, a series of hydrogen donors are screened for the reaction. As shown in Fig. 9, secondary alcohols, *e.g.* 2-propanol and 2-butanol, appear to be better hydrogen donors than primary alcohols, *e.g.* methanol and ethanol. GC–MS analysis reveals that a large amount of bulky by-products, from the self-condensation of the aldehyde or reaction of aldehyde with levulinate esters, are formed when using primary alcohols as hydrogen donors. This can be efficiently avoided by using secondary alcohols as hydrogen donors. Among all the secondary alcohols investigated, 2-proponal appears to be the best choice because its smaller kinetic diameter is good for diffusion through zeolite channels.

The recycling ability of Meso-Zr-Al-beta (100–77) and Zr-Al-beta (96–79) in the conversion of furfural to GVL is finally investigated and the results are shown in Fig. 10. No leaching of Zr or Al species into liquid phase can be detected by ICP analysis in all cases. For Zr-Al-beta catalyst, a strong catalyst deactivation is observed and the GVL yield significantly decreases from 81 to 41% after five cycles. The catalytic activity of Zr-Al-beta can be fully recovered after calcination regeneration (823 K in flowing air for 6 h), indicating the catalytic deactivation due to the deposition of bulky reagents. In contrast, no significant activity loss

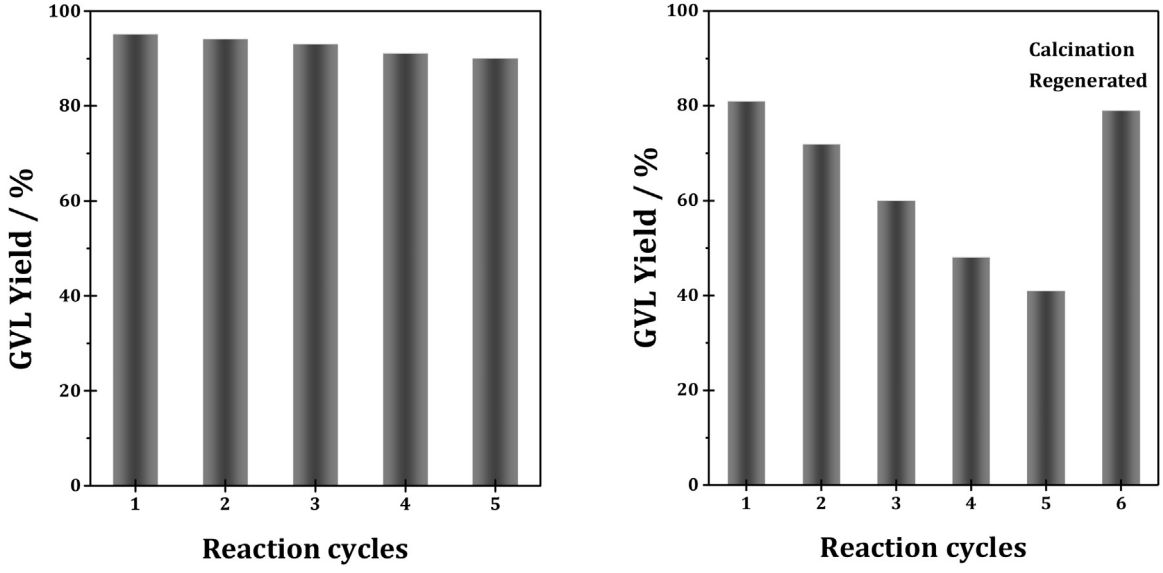

Fig. 10. Recycling test in one-pot catalytic conversion of furfural to GVL over Meso-Zr-Al-beta (100–77) (left) and Zr-Al-beta (100–79) (right). Reaction conditions: 0.12 g catalyst, 0.05 M furfural in 10 mL 2-propanol with 5% water, T = 393 K, 24 h.

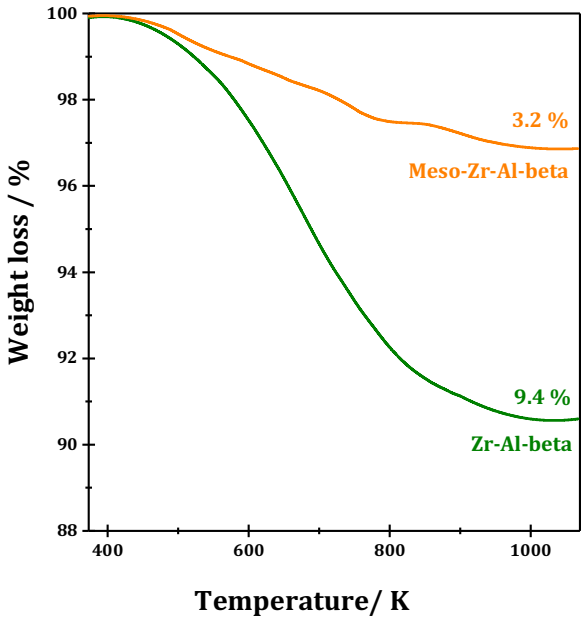

Fig. 11. TG analysis of Zr-Al-beta (96–79) and Meso-Zr-Al-beta (100–77) after furfural-to-GVL conversion for five recycles.

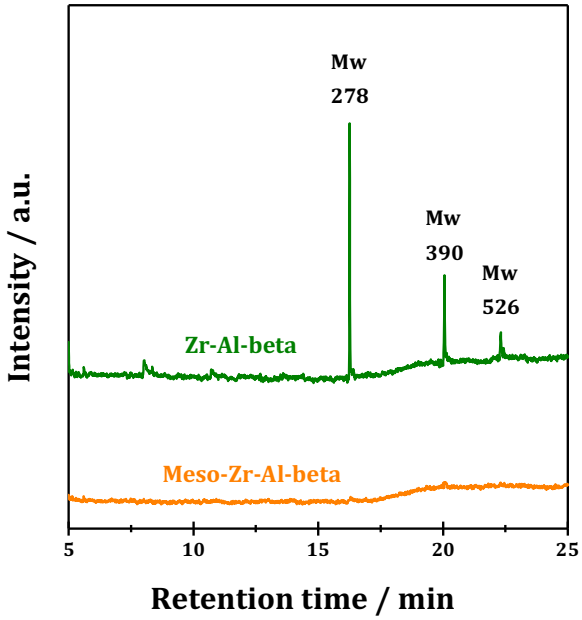

Fig. 12. GC–MS analysis of bulky organic deposits on Zr-Al-beta (96–79) and Meso-Zr-Al-beta (100–77) after furfural-to-GVL conversion for five recycles.

can be observed for Meso-Zr-Al-beta within five cycles, indicating the good recyclability of the catalyst. Obviously, the existence of hierarchical porosity in Meso-Zr-Al-beta can efficiently promote the diffusion of bulky reagents, even oligomers, and, therefore, suppress the catalyst deactivation. The good recyclability of Meso-Zr-Al-beta demonstrates its potential for practical application.

The different catalytic deactivation behaviors of Zr-Al-beta and Meso-Zr-Al-beta are further investigated by TG and dissolution-extraction analysis. As shown in Fig. 11, a small weight loss of 3.2% is observed in the temperature range of 373–1073 K for the spent Meso-Zr-Al-beta. Since a prefect carbon balance of 96% can be achieved with Meso-Zr-Al-beta in furfural-to-GVL conversion (Table 3), the weight loss should be due to organic species strongly adsorbed on the catalyst surface. While for the spent Zr-Al-beta catalyst, a three times higher weight loss of 9.4% is observed in the temperature range of 373–1073 K, corresponding to the formation of bulky organic deposits on the surface. These bulky deposits can block the catalytically active sites and/or hinder the diffusion of reactants/products, which accordingly lead to the catalytic deactivation of Zr-Al-beta in furfural-to-GVL conversion.

After a dissolution and extraction process, the nature of bulky organic deposits on the spent zeolite catalysts can be analyzed by GC–MS. No significant signals due to bulky organic species can be detected for spent Meso-Zr-Al-beta, which agrees well with the perfect carbon balance observed in the reaction (Table 3) and its good recycling ability (Fig. 10). In contrast, organic species with molecular weight (Mw) of 278, 390, and 526 are clearly observed for spent Zr-Al-beta (Fig. 12), attributed to the polymeric furfurals or furfural derivatives. Moreover, insoluble solids are also observed after the catalyst dissolution and extraction process, probably due to the formation of polymeric by-products with higher molecular weight. On the basis of these results, it can be stated that the formation of bulky organic deposits, probably polymeric furfurals or furfural derivatives, is the key reason for the catalytic deactivation of Zr-Al-beta.

3.4.2. Extended applications of Meso-Zr-Al-beta in cascade biomass conversions

In order to demonstrate the general applicability of multifunctional zeolite in biomass valorization, Meso-Zr-Al-beta is further employed as a potential catalyst in two additional cascade reactions, i.e. glucose conversion to 5-hydromethylfurfural [66–69] and trioses conversion to ethyl lactate [70,71]. As expected, an attracting 5-hydromethylfurfural productivity of 321 $g_{HMF}kg_{catalyst}^{-1}h^{-1}$ is achieved with Meso-Zr-Al-beta (49–78) at 433 K and an attracting ethyl lactate productivity of 2633 $g_{ELA}kg_{catalyst}^{-1}h^{-1}$ achieved with Meso-Zr-Al-beta (100-77) at 363 K (see **Supporting Information** for more details). In a whole, the multifunctional Meso-Zr-Al-beta is a general robust catalyst for the cascade reactions in biomass valorization.

4. Conclusions

In this study, hierarchical Meso-Zr-Al-beta zeolite has been successfully prepared via a multiple-step post-synthesis strategy with the combination of controlled dealumination, desilicication and metal ions incorporation. The physicochemical properties of Meso-Zr-Al-beta are investigated in detail and the presence of multifunctional sites, i.e. Brønsted acid sites, Lewis acid sites and hierarchical mesopores, in the single Meso-Zr-Al-beta zeolite is clearly demonstrated. Compared to the combination catalysts system of Brønsted acids and Lewis acids, the single Meso-Zr-Al-beta containing both Brønsted and Lewis acid sites should exhibit advantages in the transfer and diffusion of intermediate products in cascade reactions. The presence of mesopores can further enhance the site accessibility and increase the diffusion of reactant and products.

The as-prepared Meso-Zr-Al-beta is applied as a promising catalyst in the conversion of furfural to γ-valerolactone, a cascade reaction requiring both Brønsted and Lewis acid sites. As expected, Meso-Zr-Al-beta exhibit remarkable catalytic activity for γ-valerolactone production and good recyclability in the reaction. Typically, the highest GVL yield of 95% could be achieved after reaction for 24 h at 393 K with optimized catalyst Meso-Zr-Al-beta (100–77) and under optimized reaction conditions. The mutual compatibility of multifunctional sites, i.e. Brønsted acid sites, Lewis acid sites and mesopores, is the key to the success of the multifunctional single zeolite catalyst.

The multifunctional Meso-Zr-Al-beta zeolite could also be applied as a robust catalyst in other cascade reactions in biomass

valorization, e.g. glucose to 5-hydromethylfurfural and trioses to ethyl lactate. Similar single zeolite catalyst systems containing multiple functional sites can be designed and prepared via the strategy reported in this study, and the number of acid sites and their strength can be adjusted to derive an optimized catalyst for specific cascade reaction simply by changing the preparation parameters.

Acknowledgements

This work is financially supported by the National Natural Science Foundation of China (21373119, 21303087, 21573113, 21421001), Municipal Natural Science Foundation of Tianjin (13RCGFGX01124, 13JCQNJC05900, 14JCQNJC05700) and the Ministry of Education of China (IRT13022).

Appendix A. Supplementary data

Supplementary data associated with this article can be found, in the online version, at http://dx.doi.org/10.1016/j.apcatb.2016.12.056.

References

[1] G.W. Huber, S. Iborra, A. Corma, Chem. Rev 106 (2006) 4044–4098.
[2] A. Corma, S. Iborra, A. Velty, Chem. Rev. 107 (2007) 2411–2502.
[3] Y. Román-Leshkov, C.J. Barrett, Z.Y. Liu, J.A. Dumesic, Nature 447 (2007) 982–985.
[4] J. Jae, W. Zheng, A.M. Karim, W. Guo, R.F. Lobo, D.G. Vlachos, ChemCatChem 6 (2014) 848–856.
[5] J. Luo, H. Yun, A.V. Mironenko, K.A. Goulas, J.D. Lee, M. Monai, C. Wang, V. Vorotnikov, C.B. Murray, D.G. Vlachos, P. Fornasiero, R.J. Gorte, ACS Catal. 6 (2016) 4095–4104.
[6] H. Huang, C.A. Denard, R. Alamillo, A.J. Crisci, Y. Miao, J.A. Dumesic, S.L. Scott, H. Zhao, ACS Catal. 4 (2014) 2165–2168.
[7] A. Osatiashtiani, A.F. Lee, D.R. Brown, J.A. Melero, G. Morales, K. Wilson, Catal. Sci. Technol. 4 (2014) 333–342.
[8] W. Yu, K. Xiong, N. Ji, M.D. Porosoff, J.G. Chen, J. Catal. 317 (2014) 253–262.
[9] R. Mariscal, P. Maireles-Torres, M. Ojeda, I. Sádaba, M.L. Granados, Energy Environ. Sci. 9 (2016) 1144–1189.
[10] Y. Nakagawa, K. Takada, M. Tamura, K. Tomishige, ACS Catal. 4 (2014) 2718–2726.
[11] J.Q. Bond, D.M. Alonso, D. Wang, R.M. West, J.A. Dumesic, Science 327 (2010) 1110–1114.
[12] J. Ftouni, A. Muñoz-Murillo, A. Goryachev, J.P. Hofmann, E.J. Hensen, L. Lu, C.J. Kiely, P.C.A. Bruijnincx, B.M. Weckhuysen, ACS Catal. 6 (2016) 5462–5472.
[13] A. Corma, Chem. Rev. 97 (1997) 2373–2420.
[14] E. Taarning, C.M. Osmundsen, X. Yang, B. Voss, S.I. Andersen, C.H. Christensen, Energy Environ. Sci. 4 (2011) 793–804.
[15] M. Dusselier, P. Van Wouwe, A. Dewaele, P.A. Jacobs, B.F. Sels, Science 349 (2015) 78–80.
[16] H.Y. Luo, J.D. Lewis, Y. Román-Leshkov, Annu. Rev. Chem. Biomol. Eng. 7 (2016) 663–692.
[17] A. Corma, L.T. Nemeth, M. Renz, S. Valencia, Nature 412 (2001) 423–425.
[18] M. Moliner, Y. Román-Leshkov, M.E. Davis, Proc. Natl. Acad. Sci. 107 (2010) 6164–6168.
[19] M.S. Holm, S. Saravanamurugan, E. Taarning, Science 328 (2010) 602–605.
[20] S. Van de Vyver, C. Odermatt, K. Romero, T. Prasomsri, Y. Romaín-Leshkov, ACS Catal. 5 (2015) 972–977.
[21] E. Nikolla, Y. Román-Leshkov, M. Moliner, M.E. Davis, ACS Catal. 1 (2011) 408–410.
[22] L. Bui, H. Luo, W.R. Gunther, Y. Román-Leshkov, Angew. Chem. Int. Ed. 52 (2013) 8022–8025.
[23] S. Zhu, Y. Xue, J. Guo, Y. Cen, J. Wang, W. Fan, ACS Catal. 6 (2016) 2035–2042.
[24] T.J. Schwartz, S.M. Goodman, C.M. Osmundsen, E. Taarning, M.D. Mozuch, J. Gaskell, D. Cullen, P.J. Kersten, J.A. Dumesic, ACS Catal. 3 (2013) 2689–2693.
[25] J. Dijkmans, M. Dusselier, D. Gabriëls, K. Houthoofd, P.C. Magusin, S. Huang, Y. Pontikes, M. Trekeles, A. Vantomme, L. Giebeler, S. Oswald, B.F. Sels, ACS Catal. 5 (2015) 928–940.
[26] L. Li, J. Ding, J.G. Jiang, Z. Zhu, P. Wu, Chin. J. Catal. 36 (2015) 820–828.
[27] H.P. Winoto, B.S. Ahn, J. Jae, J. Ind. Eng. Chem. 40 (2016) 62–71.
[28] M.M. Antunes, S. Lima, P. Neves, A.L. Magalhães, E. Fazio, A. Fernandes, F. Neri, C.M. Silva, S.M. Rocha, M.F. Ribeiro, M. Pillinger, A. Urakawa, A.A. Valente, J. Catal. 329 (2015) 522–537.
[29] M.M. Antunes, S. Lima, P. Neves, A.L. Magalhães, E. Fazio, A. Fernandes, F. Neri, C.M. Silva, S.M. Rocha, M.F. Ribeiro, M. Pillinger, A. Urakawa, A.A. Valente, Appl. Catal. B 182 (2016) 485–503.
[30] M.M. Antunes, P. Neves, A. Fernandes, S. Lima, A.F. Silva, M.F. Ribeiro, C.M. Silva, M. Rillinger, A.A. Valente, Catal. Sci. Technol. 6 (2016) 7812–7829.
[31] B. Hernández, J. Iglesias, G. Morales, M. Paniagua, C. López-Aguado, J.L.G. Fierro, P. Wolf, I. Hermans, J.A. Melero, Green Chem. 18 (2016) 5777–5781.
[32] D. Verboekend, N. Nuttens, R. Locus, J. Van Aelst, P. Verolme, J.C. Groen, J. Pérez-Ramírez, B.F. Sels, Chem. Soc. Rev. 45 (2016) 3331–3352.
[33] D. Verboekend, T.C. Keller, M. Milina, R. Hauert, J. Peírez-Ramírez, Chem. Mater. 25 (2013) 1947–1959.
[34] J.C. Groen, A.A.L. Peffer, J.A. Moulijn, J. Pérez-Ramírez, Chem. Eur. J. 11 (2005) 4983–4994.
[35] J.C. Groen, T. Sano, J.A. Moulijn, J. Pérez-Ramírez, J. Catal. 251 (2007) 21–27.
[36] J. Pérez-Ramírez, D. Verboekend, A. Bonilla, S. Abelló, Adv. Funct. Mater. 19 (2009) 3972–3979.
[37] D. Verboekend, J.C. Groen, J. Pérez-Ramírez, Adv. Funct. Mater. 20 (2010) 1441–1450.
[38] D. Verboekend, T.C. Keller, S. Mitchell, J. Pérez-Ramírez, Adv. Funct. Mater. 23 (2013) 1923–1934.
[39] D. Verboekend, M. Milina, J. Pérez-Ramírez, Chem. Mater. 26 (2014) 4552–4562.
[40] J. Van Aelst, D. Verboekend, A. Philippaerts, N. Nuttens, M. Kurttepeli, E. Gobechiya, M. Haouas, A.P. Sree, J.F.M. Denayer, J.A. Martens, C.E. Kirschhock, F. Taulelle, S. Bals, G.V. Baron, P.A. Jacobs, B.F. Sels, Adv. Funct. Mater. 25 (2015) 7130–7144.
[41] S. Dzwigaj, J. Janas, J. Gurgul, R.P. Socha, T. Shishido, M. Che, Appl. Catal. B 85 (2009) 131–138.
[42] A. Srebowata, R. Baran, D. Lomot, D. Lisovytskiy, T. Onfroy, S. Dzwigaj, Appl. Catal. B 147 (2014) 208–220.
[43] B. Tang, W. Dai, X. Sun, N. Guan, L. Li, M. Hunger, Green Chem. 16 (2014) 2281–2291.
[44] B. Tang, W. Dai, G. Wu, N. Guan, L. Li, L.M. Hunger, ACS Catal. 4 (2014) 2801–2810.
[45] B. Tang, W. Dai, X. Sun, G. Wu, N. Guan, M. Hunger, L. Li, Green Chem. 17 (2015) 1744–1755.
[46] S. Song, G. Wu, W. Dai, N. Guan, L. Li, Catal. Sci. Technol. 6 (2016) 8325–8335.
[47] W. Dai, C. Wang, B. Tang, G. Wu, N. Guan, Z. Xie, M. Hunger, L. Li, ACS Catal. 6 (2016) 2955–2964.
[48] J.C. Groen, S. Abelló, L.A. Villaescusa, J. Pérez-Ramírez, Microporous Mesoporous Mater. 114 (2008) 93–102.
[49] G.G. Juttu, R.F. Lobo, Catal. Lett. 62 (1999) 99–106.
[50] B. Rakshe, V. Ramaswamy, S.G. Hegde, R. Vetrivel, A.V. Ramaswamy, Catal. Lett. 45 (1997) 41–50.
[51] L. Li, N. Guan, Microporous Mesoporous Mater. 117 (2009) 450–457.
[52] A. Ramanathan, M.C. Castro Villalobos, C. Kwakernaak, S. Telalovic, U. Hanefeld, Chem. Eur. J. 14 (2008) 961–972.
[53] M.S. Morey, G.D. Stucky, S. Schwarz, M. Fröba, J. Phys. Chem. B 103 (1999) 2037–2041.
[54] J.E. Haskouri, S. Cabrera, M. Caldés, C. Guillem, J. Latorre, A. Beltrán, D. Beltrán, M.D. Marcos, P. Amorós, Chem. Mater 14 (2002) 2637–2643.
[55] J.J. Pacheco, M.E. Davis, Proc. Natl. Acad. Sci. 111 (2014) 8363–8367.
[56] V.L. Sushkevich, I.I. Ivanova, S. Tolborg, E. Taarning, J. Catal. 316 (2014) 121–129.
[57] V.L. Sushkevich, I.I. Ivanova, E. Taarning, Green Chem. 17 (2015) 2552–2559.
[58] R. Buzzoni, S. Bordiga, G. Ricchiardi, C. Lamberti, A. Zecchina, G. Bellussi, Langmuir 12 (1996) 930–940.
[59] P. Li, G. Liu, H. Wu, Y. Liu, J.G. Jiang, P. Wu, J. Phys. Chem. B 115 (2011) 3663–3670.
[60] D.P. Langlois, H. Wolff, J. Am. Chem. Soc. 70 (1948) 2624–2626.
[61] W.R. Wright, R. Palkovits, ChemSusChem 5 (2012) 1657–1667.
[62] A.S. Amarasekara, M.A. Hasan, Catal. Commun. 60 (2015) 5–7.
[63] H. Li, Z. Fang, S. Yang, ChemPlusChem 81 (2016) 135–142.
[64] M. Chia, J.A. Dumesic, Chem. Commun. 47 (2011) 12233–12235.
[65] Z. Yang, Y.B. Huang, Q.X. Guo, Y. Fu, Chem. Commun. 49 (2013) 5328–5330.
[66] P. Carniti, A. Gervasini, F. Bossola, V.D. Santo, Appl. Catal. B 193 (2016) 93–102.
[67] J. Guo, S. Zhua, Y. Cen, Z. Qin, J. Wang, W. Fan, Appl. Catal. B 200 (2017) 611–619.
[68] X. Zhang, D. Zhang, Z. Sun, L. Xue, X. Wang, Z. Jiang, Appl. Catal. B 196 (2016) 50–56.
[69] I. Jiménez-Morales, M. Moreno-Recio, J. Pedro Maireles-Torres, A. Jiménez-López, Appl. Catal. B 164 (2015) 70–76.
[70] Y.J. Pagan-Torres, T. Wang, J.M.R. Gallo, B.H. Shanks, J.A. Dumesic, ACS Catal. 2 (2012) 930–934.
[71] K. Nemoto, Y. Hirano, K. Hirata, T. Takahashi, H. Tsuneki, K. Tominaga, K. Sato, Appl. Catal. B 183 (2016) 8–17.